Available online at www.sciencedirect.com
SCIENCE DIRECT®
Journal of Magnetic Resonance 170 (2004) 199–205
JMR Journal of Magnetic Resonance
www.elsevier.com/locate/jmr

Communication

Suppression of artifacts induced by homonuclear decoupling in amino-acid-type edited methyl ^{1}H–^{13}C correlation experiments

Hélène Van Melckebeke, Jean-Pierre Simorre, Bernhard Brutscher *

Institut de Biologie Structurale, Jean-Pierre Ebel C.N.R.S.-C.E.A.-UJF 41, rue Jules Horowitz, 38027 Grenoble Cedex, France

Received 26 May 2004; revised 24 June 2004
Available online 24 July 2004

Abstract

A detailed theoretical and experimental analysis of the artifacts induced by homonuclear band-selective decoupling during CT frequency labeling is presented. The effects are discussed in the context of an amino-acid-type editing filter implemented in ^{1}H–^{13}C CT-HSQC experiments of methyl groups in proteins. It is shown that both Bloch–Siegert shifts and modulation sidebands are efficiently suppressed by using additional off-resonance decoupling as proposed by Zhang and Gorenstein [J. Magn. Reson. 132 (1998) 81], and appropriate adjustment of a set of pulse sequence parameters. The theoretical predictions are confirmed by experiments performed on ^{13}C-labeled protein samples, yielding artifact-free amino-acid-type edited methyl spectra.

Keywords: Amino-acid-type editing; Bloch–Siegert shifts; Hadamard spectroscopy; Homonuclear decoupling; Methyl; NMR; Proteins; Resolution enhancement; Sidebands

1. Introduction

Because of their hydrophobic properties methyl groups are important probes of molecular structure and dynamics inside the core of proteins or protein complexes. The favorable relaxation properties of the ^{1}H and ^{13}C spins in methyl groups, and the availability of specific isotope-labeling strategies at the methyl positions [1,2] allow application of methyl-based NMR methods to high molecular weight systems [3–5]. In the past NMR methods focused on methyl groups have been proposed for the study of molecular structure [6–8], side chain dynamics [9,10], molecular interfaces [11,12], or ligand screening for drug design [13]. Because all these experiments are based on ^{1}H–^{13}C correlation spectra, it is crucial to have methods that provide the required high spectral resolution. We have therefore designed a pulse sequence, shown in Fig. 1A that allows amino-acid-type editing in ^{1}H–^{13}C CT-HSQC experiments of methyl groups. Amino-acid-type and ^{13}C frequency editing are both performed during the constant time (CT) delay T. The additional amino-acid-type editing filter exploits the fact that the carbon directly attached to the methyl group (C^{next}) resonates in an amino-acid-type-dependent frequency range. The C^{next} spectrum can thus be divided into four distinct bands as shown in Fig. 1B. Selective decoupling of different C^{next}-bands allows switching 'on' or 'off' the homonuclear C^{next}–C^{met} scalar coupling (J_{CC}) evolution during the CT delay T. This results in a sign change of the observed NMR signal for the corresponding methyl groups that can be exploited by a binary ('plus' and 'minus') Hadamard-type frequency encoding [14,15], according to the experimental scheme of Fig. 1C, to achieve the amino-acid-type editing.

The basic element of the amino-acid-type editing filter of Fig. 1A consists in a time period $(T + \lambda^{n} t_1)/2$ of C^{met} spin evolution in the presence of C^{next}-band-selective decoupling, followed by a 180° ^{13}C pulse, and a

* Corresponding author. Fax: +33-4-76-88-54-94.
E-mail address: Bernhard.Brutscher@ibs.fr (B. Brutscher).

1090-7807/$ - see front matter © 2004 Elsevier Inc. All rights reserved.
doi:10.1016/j.jmr.2004.06.016

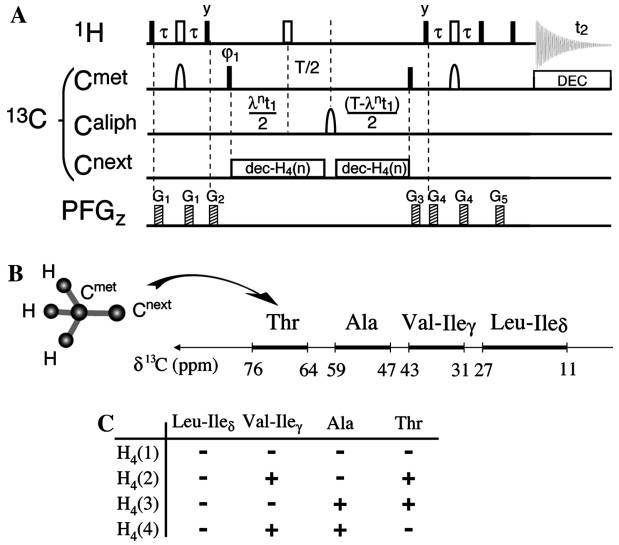

Fig. 1. Pulse sequence of the amino-acid-type edited methyl ^{1}H–^{13}C CT-HSQC. All radiofrequency (rf) pulses are applied along the x-axis unless indicated. 90° and 180° rf pulses are represented by filled and open pulse symbols, respectively. The proton carrier is set to the water resonance (4.7 ppm), and the ^{13}C carrier to the center of the methyl region (19 ppm) throughout the experiment. ^{13}C pulses drawn on the C^{aliph} or C^{next} lines are frequency shifted to 35 ppm (C^{aliph}) and the center of the corresponding C^{next} bands, respectively, by a linear phase ramp. The selective 180° C^{met} pulses are applied with an i-SNOB-5 shape [22] covering a bandwidth of 18 ppm. For application at high magnetic field strengths, an offset-compensating C^{aliph} refocusing pulse $58_x - 140_{-x} - 344_x - 140_{-x} - 58_x$ [23] is used during the CT delays T in order to properly invert all C^{met} and C^{next} carbon spins over a bandwidth of 80 ppm. The CT delay was set to $T = 28$ ms, and the INEPT transfer delays to $\tau = 1.6$ ms. ^{13}C decoupling during acquisition is achieved using a WALTZ-16 sequence [24] at a field strength of $\gamma B_1/2\pi = 3$ kHz. Pulsed field gradients, G_1–G_5 are applied along the z-axis (PFG_z) with a gradient strength of approximately 20 G/cm and lengths ranging from 100 to 500 μs, followed by a recovery delay of 100 μs. The phase cycle employed is $\varphi_1 = x, -x$, and $\varphi_{rec} = x, -x$. Quadrature detection in t_1 is obtained by incrementing the phase φ_1 according to STATES-TPPI. Constant-adiabaticity (CA) WURST-2 pulses are used as the basic elements for the C^{next}-decoupling. The CA-WURST-2 pulses have a length of $\tau_p = 5$ ms and cover a bandwidth of 12 ppm. They are centered at 37 ppm (1 ppm), 53 ppm (−15 ppm), and 70 ppm (−32 ppm) for the Val-Ile-γ, Ala, and Thr C^{next}-bands, respectively (B). The values in parentheses indicate the center of the symmetric off-resonance decoupling applied for each band using the same amplitude modulation but opposite frequency sweep [17]. Multiple-band-selective decoupling is achieved by vector addition of the individual WURST pulses [25]. The final decoupling sequence is phase cycled according to a TPG-5 supercycle [26]. The C^{next}-decoupling is restarted at the beginning of the decoupling waveform after the 180° C^{aliph} refocusing pulse. For the four-step Hadamard amino-acid-type selection filter, four experiments are recorded using C^{next}-decoupling of the bands indicated by a 'plus' in (C). A Hadamard transformation [14,15] is applied along the filter dimensions to disentangle the NMR signals from the individual frequency bands.

second time period $(T - \lambda^n t_1)/2$ of C^{met} spin evolution in the presence of C^{next}-band-selective decoupling. For the following discussion we will ignore the scaling factors ($\lambda^n = 1$). Homonuclear decoupling induces a number of undesired side effects, such a Bloch–Siegert frequency shifts and modulation sidebands [16]. Or, it is crucial for the performance of the present amino-acid-type editing filter, which relies on the addition and subtraction of different sub-spectra, that Bloch–Siegert shifts are absent from the spectrum. Otherwise anti-phase-like residual peaks will be observed due to incomplete peak cancelation. Modulation sidebands give rise to spurious artificial peaks, which may interfere with real cross-peaks, making the analysis of complex spectra difficult. We have thus undertaken a detailed theoretical and experimental analysis of the effects of multiple-band-selective C^{next} decoupling on the C^{met} spectrum, in order to devise appropriate pulse schemes to minimize or compensate these undesired peak shifts and sidebands.

If for each C^{next} band a second decoupling field is applied, symmetrically with respect to the center of the methyl spectrum with the same amplitude modulation $f(t)$ and opposite frequency sweep [17], spin evolution in the rotating frame is governed by a time-dependent first-order average Hamiltonian $H^{(1)}(t)$, as demonstrated by Zhang and Gorenstein [18]:

$$H^{(1)}(t) = \alpha f_{rms}^2(t) I_z \tag{1}$$

with

$$\alpha = -2\pi \frac{v}{\Delta v_{rf}^2} \tag{2}$$

and

$$f_{rms}^2(t) = \frac{1}{t}\int_0^t f^2(\tau)\,d\tau, \tag{3}$$

where Δv_{rf} is the difference of the average decoupling frequency and the spectral center frequency, and v is the frequency offset of a given spin from the spectral center.

The evolution of the spin density operator $\sigma(t)$ during the CT delay T in the sequence of Fig. 1A is then schematically described by:

$$\sigma(0) \overset{H^{(1)}(t)}{\rightarrow} \sigma((T+t_1)/2) \overset{\pi I_x}{\rightarrow} \overset{H^{(1)}(t)}{\rightarrow} \sigma(T), \tag{4}$$

which can be simplified to

$$\sigma(0) \overset{H^{(1)}(t)}{\rightarrow} \sigma((T+t_1)/2) \overset{-H^{(1)}(t)}{\rightarrow} \sigma(T). \tag{5}$$

We can now introduce a phase modulation function $\theta(t_1, T)$ defined as follows:

$$\sigma(T) = \exp\{-i\theta(t_1,T)I_z\}\sigma(0)\exp\{+i\theta(t_1,T)I_z\}. \tag{6}$$

From Eqs. (1), (5), and (6) we obtain the following expression for the phase modulation function $\theta(t_1, T)$:

$$\theta(t_1,T) = \alpha\left[\int_0^{\frac{T+t_1}{2}} f^2(\tau)\,d\tau - \int_0^{\frac{T-t_1}{2}} f^2(\tau)\,d\tau\right] = \alpha\int_{\frac{T-t_1}{2}}^{\frac{T+t_1}{2}} f^2(\tau)\,d\tau. \tag{7}$$

Eq. (7) takes into account that the decoupling waveform is restarted at the beginning of the decoupling waveform after the 180° C^{aliph} refocusing pulse (see Fig. 1A).

For the amino-acid-type editing filter of Fig. 1A, a constant-adiabaticity WURST-2 pulse shape [19] is chosen as the repeated element of the decoupling sequence for its relatively sharp inversion profile and the moderate radiofrequency (rf) power required. For this special case of WURST-2 decoupling the amplitude modulation function is given by

$$f(t) = f_{\max}\sin^2\left(\pi\frac{t}{\tau_p}\right) \tag{8}$$

with τ_p the length of a single WURST pulse and $f_{\max}$ the peak amplitude of the rf field. For WURST-2 decoupling, the integral in Eq. (7) can be evaluated analytically, and we obtain the following phase modulation function

$$\theta(t_1,T) = \omega_{BS}t_1 - a\cos\left(\pi\frac{T}{\tau_p}\right)\sin\left(\pi\frac{t_1}{\tau_p}\right) + \frac{a}{8} \times \cos\left(2\pi\frac{T}{\tau_p}\right)\sin\left(2\pi\frac{t_1}{\tau_p}\right) \tag{9}$$

with the coefficients $\omega_{BS} = -\frac{3\pi}{4}\frac{f_{\max}^2}{\Delta\nu_{rf}^2}\nu$, and $\alpha = -\frac{f_{\max}^2}{\Delta\nu_{rf}^2}\nu\tau_p$.

1.1. Bloch–Siegert shift compensation

The first term in Eq. (9) gives rise to a Bloch–Siegert shift $\Delta\nu_{BS}$ with $\omega_{BS} = 2\pi\Delta\nu_{BS}$. If we introduce the root-mean square rf amplitude f_{rms} for the WURST-2 decoupling sequence defined as

$$f_{rms} = f_{rms}(\tau_p) = \sqrt{\frac{1}{\tau_p}\int_0^{\tau_p} f^2(\tau)\,d\tau} = \sqrt{\frac{3}{8}}f_{\max}, \tag{10}$$

we obtain an expression for the Bloch–Siegert shift which is well known for the case of homonuclear decoupling during real-time frequency labeling [17]

$$\Delta\nu_{BS} = -\left(\frac{f_{rms}}{\Delta\nu_{rf}}\right)^2\nu. \tag{11}$$

The two decoupling fields applied symmetrically with respect to the center of the observed spectrum with the same shape and opposite frequency sweep, induce a Bloch–Siegert shift $\Delta\nu_{BS}$ which is, within a certain frequency range, a linear function of the frequency offset ν. Therefore, Bloch–Siegert shift compensation in this linear regime is achieved by using a dilated evolution time $\lambda^n t_1$ (see Fig. 1A) with the scaling factor λ^n set to

$$\lambda^n = 1 + (f_{rms}/\Delta\nu_{rf})^2. \tag{12}$$

The use of additional symmetric off-resonance decoupling, and appropriate scaling factors λ^n compensates the Bloch–Siegert shifts, and ensures identical peak positions along the ^{13}C frequency dimension.

We have experimentally evaluated the Bloch–Siegert shifts as a function of the chemical shift offset ν and the magnetic field strength B_0. Bloch–Siegert shifts, measured for the two small proteins, *human* ubiquitin (76 residues) and *Ralstonia metallidurans* MerAa (68 residues), are plotted in Fig. 2 as a function of the C^{met} chemical shift. CT-HSQC spectra were recorded at Varian INOVA 800 and INOVA 600 spectrometers using the pulse sequence of Fig. 1A. The Bloch–Siegert shifts were extracted from the relative cross-peak positions along the ^{13}C dimension in the spectra acquired with and without band-selective C^{next}-decoupling, and the scaling factors set to $\lambda^n = 1$ for all experiments. For the spectra recorded with simultaneous Ala and Thr C^{next}-decoupling the observed offset dependence is well described by Eq. (11), and the scaling factors calculated from Eq. (12) thus provide a good estimate of the required correction. For experiments with C^{next}-decoupling of the (Val-Ile$_\gamma$) band, however, a deviation from linearity is observed (Figs. 2A and C). This band is closest to the observed methyl ^{13}C, and thus responsible for most of the spectral perturbation. For optimal filter performance over the methyl ^{13}C bandwidth, it is therefore necessary to experimentally optimize the scaling factors λ^n, taking into account the non-linear behavior of the observed Bloch–Siegert shifts. Because the Bloch–Siegert shifts depend on the B_0-field strength, a different set of scaling factors λ^n has to be used for different magnetic fields. For the application presented here, we have empirically optimized the following scaling factors: $\lambda^2_{600} = 1.0046$, $\lambda^3_{600} = 1.0181$, and $\lambda^4_{600} = 1.0162$ at 600 MHz, and $\lambda^2_{800} = 1.0028$, $\lambda^3_{800} = 1.0102$, and $\lambda^4_{800} = 1.0091$ at 800 MHz, which yield residual Bloch–Siegert shifts of less than 1.0 Hz within a spectral width of about 15 ppm (Figs. 2B and D). Outside this spectral range the frequency shift increases very quickly, and as a consequence the filter performance decreases. The ^{13}C frequency range of 11.5–26.5 ppm, however, covers the large majority of methyl resonances (≈90% of the methyls in the BMRB). We conclude from these results that a similar Bloch–Siegert shift-compensation performance is obtained for experiments conducted at currently available high magnetic field strengths (400–900 MHz ^1H frequency), using the pulse sequence of Fig. 1A and optimized scaling factors λ^n.

1.2. Modulation sideband suppression

The periodic amplitude-modulated decoupling field also induces cyclic irradiation sidebands, commonly referred to as *modulation sidebands* [16]. These sidebands are described by the second and third terms of Eq. (9), which correspond to first- and second-order harmonic phase modulations in the rotating frame. Similar to the Bloch–Siegert shifts, a linear offset dependence is obtained. This leads to sideband suppression for all C^{met}

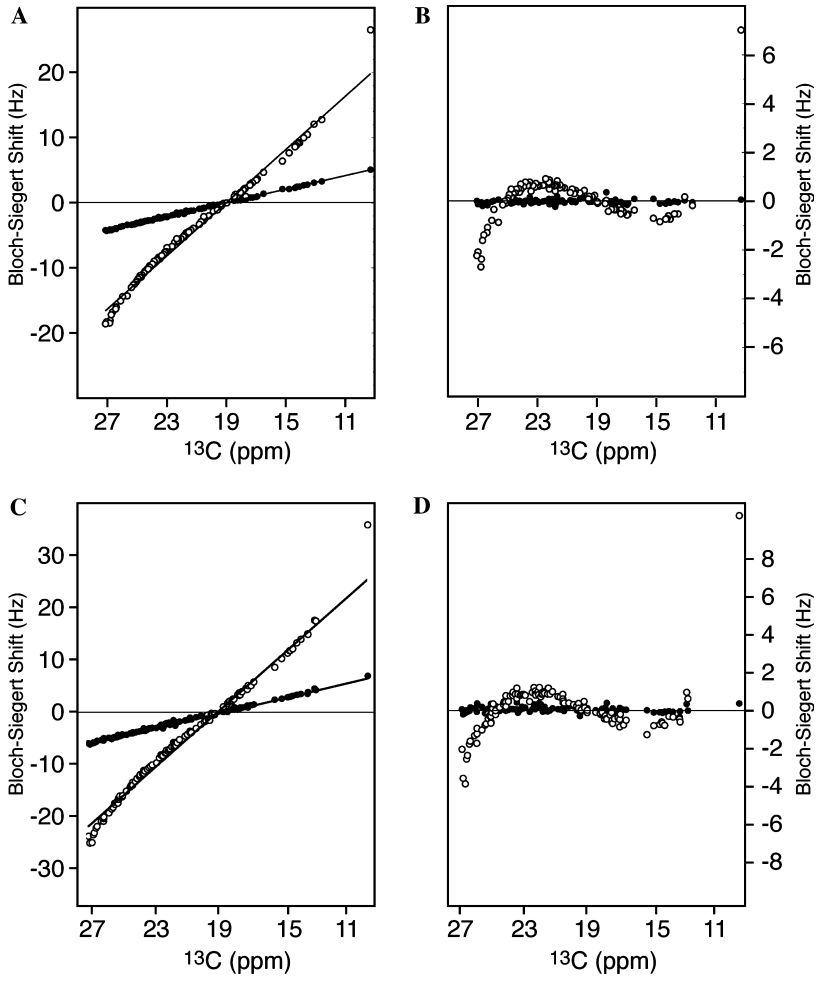

Fig. 2. Bloch–Siegert shifts measured at 800 MHz (A) and at 600 MHz (C) ^{1}H frequency with the pulse sequence of Fig. 1A setting $\lambda^n = 1$. Open circles correspond to measurements with simultaneous C^{next}-decoupling of the Ala and (Val-Ile-γ) bands, and filled circles represent the corresponding results for Ala and Thr C^{next}-decoupling. Residual Bloch–Siegert shifts using optimized scaling factors λ^n are plotted in (B) for 800 MHz ($\lambda^1_{800} = 1.0$, $\lambda^2_{800} = 1.0026$, $\lambda^3_{800} = 1.0102$, $\lambda^4_{800} = 1.0091$), and in (D) for 600 MHz ($\lambda^1_{600} = 1.0$, $\lambda^2_{600} = 1.0046$, $\lambda^3_{600} = 1.0181$, $\lambda^4_{600} = 1.0162$).

resonances close to the spectral center. Far from the center, first- and second-order sidebands are predicted with an eight-times higher intensity for the first-order sidebands. In the following, we will focus on the larger first-order effects, which are observable at frequencies $\nu_{\pm 1} = \nu_0 \pm 1/(2\tau_p)$, with ν_0 the central peak frequency and τ_p the periodicity of the decoupling sequence. Interestingly, a periodic modulation of the sideband amplitudes $A_{\pm 1}$ with the CT delay T is predicted from Eq. (9), $A_{\pm 1} \propto \pm\cos(\pi T/\tau_p)$, yielding sideband suppression by adjusting the constant time delay T and the decoupling pulse length τ_p in such a way that

$$\frac{T}{\tau_p} = \frac{(2m-1)}{2} \tag{13}$$

with m an integer.

To confirm these theoretical results we have recorded a series of methyl CT ^{1}H–^{13}C correlation spectra of *human* ubiquitin at an INOVA 800 spectrometer using the pulse sequence of Fig. 1A with simultaneous C^{next}-decoupling of the Ala and (Val-Ile$_\gamma$) bands, as well as symmetric off-resonance decoupling. Spectra were recorded for two different WURST-2 pulse lengths of $\tau_p = 3$ ms and $\tau_p = 5$ ms, and a series of CT delays T in the range $26\,\text{ms} \leqslant T \leqslant 33\,\text{ms}$. A single cross-peak extracted at a C^{met} frequency of 26.9 ppm is shown in Figs. 3A and B to highlight the position and intensity of the detected modulation sidebands. Only first-order sidebands are observed in the spectra of Fig. 3 located 167 (Fig. 3A) and 100 Hz (Fig. 3B) away from the central peak, which exactly corresponds to the predicted frequencies of $\nu_{\pm 1} = \nu_0 \pm 1/(2\tau_p)$. The observed asymmetry of the sideband intensity is explained by the fact that the harmonic phase modulation in the rotating frame also yields a small symmetric contribution to the sideband intensity, which adds to one sideband and subtracts from the other one [18]. The intensity modulation as a function of the CT delay T is confirmed by the experimental results shown in Fig. 3. As expected from our theoretical treatment, the sideband intensities are modulated with

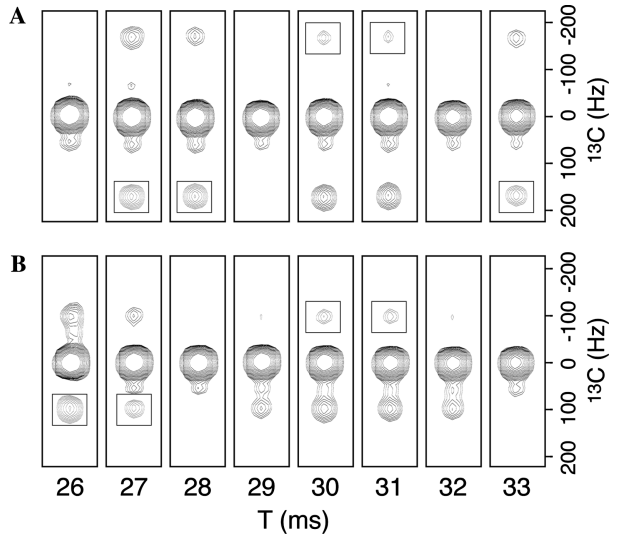

Fig. 3. Small spectral region extracted from a CT-HSQC methyl ^{1}H–^{13}C correlation spectra of ubiquitin recorded at 800 MHz ^{1}H frequency using the pulse sequence of Fig. 1A. C^{next}-decoupling of the Ala and (Val-Ileγ) bands is applied during the CT time delay T, which is varied from 26 to 33 ms. The experiments were repeated for a WURST pulse length of (A) $\tau_p = 3$ ms, and (B) $\tau_p = 5$ ms. A single methyl peak is observed in the plotted spectral region extracted at $\omega_C = 26.9$ ppm. A box indicates a peak with negative intensity.

a periodicity of τ_p. Therefore first-order sideband suppression is achieved over the whole C^{met} spectral range by properly adjusting the constant time delay T and the decoupling pulse length τ_p. If we consider the additional experimental conditions $\tau_p < 1/5J_{CC}$ and $T \approx 1/J_{CC}$ ($J_{CC} \approx 35$ Hz), the optimal parameter combination is found to be $T = 28$ ms and $\tau_p = 5$ ms for the amino-acid-type editing filter of Fig. 1A. Note that the experimentally optimized ratio $T/\tau_p = 5.6$ slightly deviates from the theoretical value $T/\tau_p = 5.5$ predicted by Eq. (13).

Other experimental schemes for the suppression of sidebands induced by homonuclear decoupling have been presented before [18,20]. The common idea of these approaches is to average out the modulation of the effective magnetic field in the rotating frame by shifting the origin of the decoupling waveform for different scans. This contrasts with the method presented here, where sideband suppression is achieved in a 'single scan' by exploiting the inherent properties of homonuclear decoupling during constant time spin evolution. This result is not limited to the particular case of WURST-2-based decoupling sequences. For the general case of an amplitude-modulated waveform, which can be decomposed into a Fourier series, one obtains after integration in Eq. (7) terms of the form

$$k_1^n \left\{ k_2^n \sin\left(\frac{n}{2}\pi\frac{T}{\tau_p}\right) + k_3^n \cos\left(\frac{n}{2}\pi\frac{T}{\tau_p}\right) \right\} \sin\left(\frac{n}{2}\pi\frac{t_1}{\tau_p}\right)$$

in the phase modulation function $\theta(t_1, T)$, with n an integer, and k_1^n, k_2^n, and k_3^n constants depending on the chosen waveform. It is thus still possible to suppress the dominant term yielding the highest sideband intensity by adjusting the ratio T/τ_p.

1.3. Experimental application of methyl amino-acid-type editing

For amino-acid-type editing in the pulse sequence of Fig. 1A, four experiments $H_4(1)$, $H_4(2)$, $H_4(3)$, and $H_4(4)$ are performed with simultaneous decoupling of different C^{next} bands (Fig. 1B) indicated by a 'plus' in the scheme of Fig. 1C. In addition, 'off'-resonance decoupling is applied for each C^{next} band symmetrically to the C^{met} spectral center. The use of different B_0-field-dependent scaling factors λ^n for the four experiments ensures identical peak positions along the ^{13}C dimension. Note that the correction factors λ^n are additive for the different C^{next} bands, and that they have been optimized experimentally as explained above. A Hadamard transformation [14], instead of a Fourier transformation, then allows disentangling the four bands along the additional amino-acid-type dimension. This yields a $(2_{cs} + 1_{aa})$-D methyl correlation spectrum, with two chemical shift and one amino-acid-type dimensions.

An example of an amino-acid-type edited methyl ^{1}H–^{13}C correlation spectrum, recorded using the pulse sequence of Fig. 1A, is shown in Fig. 4. The data were acquired at 800 MHz ^{1}H frequency on a sample of uniformly ^{13}C-, ^{15}N-labeled calmodulin, a 163-residue protein with 90 methyl groups that has been extensively studied by NMR in the past. The four 2D ^{1}H–^{13}C spectra, plotted in Figs. 4A–D, were extracted along the amino-acid-type dimension of the $(2_{cs} + 1_{aa})$-D methyl correlation spectrum. Overall, the spectra are artifact-free, and the different C^{next} frequency bands are well separated in the four spectra. Some cross-talk is observed between the Leu and Val peaks, for which the actual C^{next} frequency ranges slightly overlap. Therefore some Val peaks (Fig. 4C) are also detected in the spectrum of Fig. 4A, although with a significantly lower intensity. The methyl group at C^{ε} position of methionine side chains, which has no directly attached carbon, gives rise to a negative cross-peak in the subspectrum shown in Fig. 4A. The amino-acid-type editing filter enhances spectral resolution, and allows additional amino-acid-type identification for the purpose of resonance assignment. Many NMR experiments, based on the spectral resolution of ^{1}H–^{13}C methyl correlation spectra, may be improved by the use of additional amino-acid-type editing. Recently, we have demonstrated that amino-acid-type editing in methyl NOESY experiments helps for unambiguous NOE peak assignment, and allows fast acquisition of methyl NOE data [21]. Other potential applications

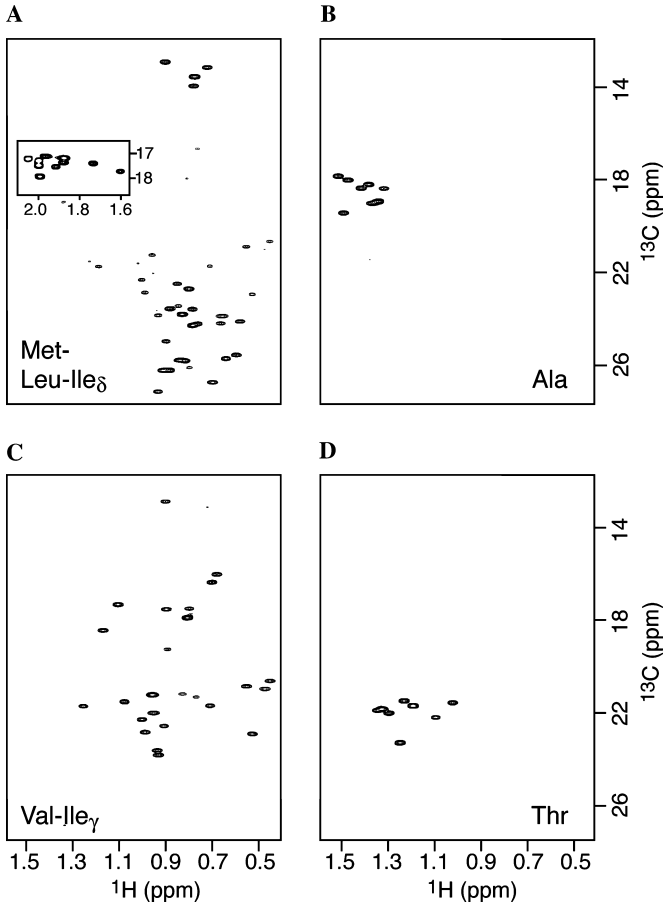

Fig. 4. Amino-acid-type edited methyl CT-HSQC spectrum recorded at 800 MHz ^{1}H frequency using the pulse sequence of Fig. 1A on a sample of ^{13}C-labeled calmodulin (1 mM, 27 °C, pH 6.5). $4(H_4) \times 110(^{13}C) \times 512(^1H)$ complex points were recorded for spectral widths of 4000 Hz (^{13}C) and 9000 Hz (^{1}H) in an overall experimental time of 2 h. The four ^{1}H–^{13}C spectra are extracted along the amino-acid-type dimension. They show methyl cross-peaks from (A) Met-Leu-Ile$_\delta$, (B) Ala, (C) Val-Ile$_\gamma$, and (D) Thr residues. The methionine cross-peaks in the inset of (A) have negative intensity.

of this filter include the study of side chain dynamics by ^{13}C or ^{2}H spin relaxation measurements, the quantification of spin–spin couplings, and the study of molecular interfaces by chemical shift mapping.

In summary, we have shown that both, Bloch–Siegert shifts and cyclic irradiation sidebands induced by symmetric band-selective decoupling during CT frequency labeling can be suppressed by the use of a dilated evolution time λt_1, and proper adjustment of the T/τ_p ratio. This has allowed us to design a filter sequence based on multiple-band-selective homonuclear decoupling, which yields clean amino-acid-type editing in methyl ^{1}H–^{13}C correlation experiments of proteins. Other NMR experiments may benefit as well from artifact-free band-selective homonuclear decoupling during CT frequency labeling. Examples include base-type editing in HCN- or HCC-type experiments of nucleic acids, and C^β-decoupling during C^α frequency labeling in HNCACO-type experiments of proteins. The implementation of such experimental schemes is currently under investigation in our laboratory.

Acknowledgments

This work was supported by the Commissariat à l'Energie Atomique and the Centre National de la Recherche Scientifique. The authors thank B. Bersch, J. Covès, D. Bouvier, and P. Gans for the preparation of the labeled protein samples. H.V.M. acknowledges the receipt of a fellowship from the C.E.A.

References

[1] K.H. Gardner, L.E. Kay, The use of ^{2}H, ^{13}C, ^{15}N multidimensional NMR to study the structure and dynamics of proteins, Annu. Rev. Biophys. Biomol. Struct. 27 (1998) 357–406.

[2] N.K. Goto, K.H. Gardner, G.A. Mueller, R.C. Willis, L.E. Kay, A robust and cost-effective method for the production of Val, Leu, Ile(δ1) methyl-protonated ^{15}N-, ^{13}C-, ^{2}H-labeled proteins, J. Biomol. NMR 13 (1999) 369–374.

[3] K.H. Gardner, M.K. Rosen, L.E. Kay, Global folds of highly deuterated, methyl-protonated proteins by multidimensional NMR studies, Biochemistry 36 (1997) 1389–1401.

[4] V. Tugarinov, L.E. Kay, Ile, Leu, and Val methyl assignment of the 723-residue malate synthase G using a new labeling strategy and novel NMR methods, J. Am. Chem. Soc. 125 (2003) 13868–13878.
[5] V. Tugarinov, P.M. Hwang, J.E. Ollerenshaw, L.E. Kay, Cross-correlated relaxation enhanced ^{1}H–^{13}C NMR spectroscopy of methyl groups in very high molecular weight proteins and protein complexes, J. Am. Chem. Soc. 125 (2003) 10420–10428.
[6] M.K. Rosen, K.H. Gardner, R.C. Willis, W.E. Parris, T. Pawson, L.E. Kay, Selective methyl group protonation of perdeuterated proteins, J. Mol. Biol. 263 (1996) 627–636.
[7] W.J. Metzler, M. Wittekind, V. Goldfarb, L. Mueller, B.T. Farmer, Incorporation of ^{1}H-^{13}C-^{15}N-{Ile, Leu, Val} into a perdeuterated, ^{15}N-labeled protein: potential in structure determination of large proteins by NMR, J. Am. Chem. Soc. 118 (1996) 6800–6901.
[8] G.A. Mueller, W.Y. Choy, D. Yang, J.D. Forman-Kay, R.A. Venters, L.E. Kay, Global folds of proteins with low densities of NOEs using residual dipolar couplings: application to the 370-residue maltodextrin-binding protein, J. Mol. Biol. 300 (2000) 197–212.
[9] R. Ishima, J.M. Louis, D.A. Torchia, Transverse ^{13}C relaxation of CHD_2 methyl isotopmers to detect slow conformational changes of protein side chains, J. Am. Chem. Soc. 121 (1999) 11589–11590.
[10] O. Millet, D.R. Muhandiram, N.R. Skrynnikov, L.E. Kay, Deuterium spin probes of side-chain dynamics in proteins. 1. measurement of five relaxation rates per deuteron in ^{13}C-labeled and fractionally ^{2}H-enriched proteins in solution, J. Am. Chem. Soc. 124 (2002) 6439–6448.
[11] E.F. DeRose, T. Darden, S. Harvey, S. Gabel, F.W. Perrino, R.M. Schaaper, R.E. London, Elucidation of the epsilon–theta subunit interface of *Escherichia coli* DNA polymerase III by NMR spectroscopy, Biochemistry 42 (2003) 3635–3644.
[12] W.P. Shao, S.C. Im, E.R.P. Zuiderweg, L. Waskell, Mapping the binding interface of the cytochrome *b*(5)–cytochrome *c* complex by nuclear magnetic resonance, Biochemistry 42 (2003) 14774–14784.
[13] P.J. Hajduk, D.J. Augeri, J. Mack, R. Mendoza, J. Yang, S.F. Betz, S.W. Fesik, NMR-based screening of proteins containing ^{13}C-labeled methyl groups, J. Am. Chem. Soc. 122 (2000) 7898–7904.
[14] J. Hadamard, Résolution d'une question relative aux déterminants, Bull. Sci. Math. 17 (1893) 240–248.
[15] E. Kupce, T. Nishida, R. Freeman, Hadamard NMR spectroscopy, Prog. NMR Spectrosc. 42 (2003) 95–122.
[16] E. Kupce, H. Matsuo, G. Wagner, Homonuclear decoupling in proteins, Biol. Magn. Reson. 16 (1999) 149–193.
[17] S. Zhang, D.G. Gorenstein, Bloch-Siegert shift compensated and cyclic irradiation sidebands eliminated, double-adiabatic homonuclear decoupling for ^{13}C- and ^{15}N-double-labeled proteins, J. Magn. Reson. 132 (1998) 81–87.
[18] S. Zhang, D.G. Gorenstein, "BEST" homonuclear adiabatic decoupling for ^{13}C- and ^{15}N-double-labeled proteins, J. Magn. Reson. 138 (1999) 281–287.
[19] E. Kupce, R. Freeman, Optimized adiabatic pulses for wideband spin inversion, J. Magn. Reson. A 118 (1996) 299–303.
[20] J. Weigelt, A. Hammarström, W. Bermel, G. Otting, Removal of zero-quantum coherence in protein spectra using SESAM decoupling and suppression of decoupling sidebands, J. Magn. Reson. B 110 (1996) 219–224.
[21] H. Van Melckebeke, J.-P. Simorre, B. Brutscher, Amino acid-type edited NMR experiments for methyl–methyl distance measurements in ^{13}C-labeled proteins, J. Am. Chem. Soc. (2004) (in press).
[22] E. Kupce, J. Boyd, I.D. Campbell, Short selective pulses for biochemical applications, J. Magn. Reson. B 106 (1995) 300–303.
[23] A.J. Shaka, A.J. Pines, Symmetric phase-alternating composite pulses, Magn. Reson. 71 (1987) 495–503.
[24] A.J. Shaka, J. Keeler, T. Frenkiel, R. Freeman, An improved sequence for broadband decoupling: Waltz-16, J. Magn. Reson. 52 (1983) 335–338.
[25] E. Kupce, R. Freeman, Techniques for multisite excitation, J. Magn. Reson. A 105 (1993) 234–238.
[26] R. Tycko, A. Pines, R. Gluckenheimer, Fixed point theory of iterative excitation schemes in NMR, J. Chem. Phys. 83 (1985) 2775–2802.